Journal of Sound and Vibration (2001) **247**(3), 489–508
doi:10.1006/jsvi.2001.3756, available online at http://www.idealibrary.com on IDEAL®

A CRUDE METHOD OF LOOP-SHAPING ADAPTIVE STRUCTURES THROUGH OPTIMUM SPATIAL COMPENSATOR DESIGN

G. C. Smith and R. L. Clark

Department of Mechanical Engineering and Materials Science, Duke University, Durham, NC 27708-0302, *U.S.A. E-mail: rclark@duke.edu*

(*Received* 13 *December* 1999, *and in final form* 17 *April* 2001)

This work continues the development of methods for optimum spatial compensator design of adaptive structures and is based upon the use of a computationally efficient estimate of the Hankel singular values of the open-loop controllability and observability Gramians to form the design metric. Results demonstrate that when a range of transducer sizes is considered in the candidate set, the proper spatial compensator design metric is the product of a coupling cost and a de-coupling cost. This leads to designs that provide a balance between coupling to modes that are important for control and de-coupling from modes not important for control. As demonstrated on a simply supported plate structure, the optimum design resulting from the application of the approach detailed herein significantly limits coupling to all modes except those present in the performance metric. The method provides the ability to crudely loop-shape the adaptive structure, as demonstrated through modification of both the actuator-to-sensor frequency response function and the system loop gain. It is concluded that emphasis should be placed on designing spatial compensators in order to facilitate the design of controllers for adaptive structures.

1. INTRODUCTION

Adaptive structures have demonstrated the potential to outperform conventional structures in a number of different areas [1]. The most common example is the suppression of low-frequency vibration and sound, where active control techniques are known to surpass traditional passive methods [2, 3] and the application and use of adaptive structures is just beginning. This paper investigates techniques to design adaptive structures for increased performance and robustness.

In an adaptive structure, the control system modifies the dynamic response of the structure to external disturbances and/or varying environmental conditions. The process of designing a control system to meet desired objectives is known as *compensation* and current approaches to optimum compensator design usually involve frequency shaping the system open- and closed-loop transfer functions. Traditionally, compensator design techniques have been based solely upon optimization of the controller to meet the most important design objectives. The controller can also be called the *temporal compensator* of the system; recognizing that the action of the controller is to modify the temporal response of the sensor signals to form the proper control inputs signals.

Work in adaptive structures has shown that optimum compensator design may be augmented by considering the design of the *spatial compensator* [1] of the system. Spatial compensation is defined as the influence of the type, shape, size, and placement of the

0022-460X/01/430489 + 20 $35.00/0

transducers on the open-loop response and, as a result, the closed-loop temporal compensator design. Further, the control system of the adaptive structure is a combination of both the temporal and spatial compensator designs.

The optimization of actuator and sensor placement has been previously demonstrated as important to control with adaptive structures [1, 4, 5]. Optimum transducer placement yields greater performance with less control effort and hardware [6]. Recently, Clark and Cox [7] and Smith and Clark [8] have presented techniques to also increase system robustness by optimizing transducer placement. Increased system robustness is defined in reference [7] as reduced coupling to out-of-bandwidth modes, where model fidelity frequently suffers. Smith and Clark [8] reduced coupling to both the out-of-bandwidth modes and the in-bandwidth modes pre-selected by the control system designer as not important for control. The design approach leads to reduced model and controller order. Similar approaches to optimum actuator and sensor placement for increased system performance were first presented by Lim [9]. The design techniques discussed in references [7–9] are computationally efficient and allow rapid optimization of the spatial compensator design of an adaptive structure. These design approaches are based upon open-loop estimates of the controllability and observability Gramians of the system.

The objective of this work is to continue the development of techniques for optimum spatial compensator design. The design metric introduced in section 2 is an advancement of the open-loop approaches developed in references [7–9]. This design metric is formed as the product of a coupling cost and a de-coupling cost. Analysis is presented which demonstrates the necessity of this approach when one considers transducers of varying size. The design metric is then applied to vibration control of a simply supported plate with one piezoelectric sensor and one piezoelectric actuator. A SISO pair is chosen since the optimum design should reflect the minimum number of inputs and outputs required to meet the adaptive structure objectives. The properties of the analytical plate are given in section 3. Results of this approach are presented in section 4. The results demonstrate that the design metric leads to a crude method of loop-shaping adaptive structures by optimum spatial compensator design. The conclusions of this work are given in section 5.

2. THEORY

Discussion of optimum spatial compensator design for adaptive structures begins with a description of the test structure. In this case, an analytical model of a simply supported plate is developed; the simplicity of a plate structure allows one to focus on the influence of the design technique versus characteristics of the structural dynamics. The open-loop design metric is then presented and based upon an estimate of the Hankel singular values (HSVs) to provide a measure of both performance and robustness. Finally, the $\mathscr{H}_2$ control design process is discussed, as used to design the optimum temporal compensator, i.e., controller, for the adaptive structure.

2.1. PLATE MODEL

The simply supported plate structure is modelled using the assumed-modes method [1]. It is assumed that the plate transverse displacement, $r(x, y, t)$, can be represented by a finite series of the *in vacuo* eigenfunctions of the form

$$r(x, y, t) = \sum_{n=1}^{N_m} \phi_n(x, \ y) q_n(t) = \sum_{n=1}^{N_m} \sin\left(\frac{n_x \pi x}{L_x}\right) \sin\left(\frac{n_y \pi y}{L_y}\right) q_n(t), \tag{1}$$

where N_m is the number of structural modes in the model, (n_x, n_y) is the indice pair for $\phi_n(x, y)$, L_x is the plate width, L_y is the plate height, and $q_n(t)$ is the generalized displacement. Substituting equation (1) into the partial differential equation for the plate leads to a set of ordinary differential equations of the form

$$\ddot{q}_n(t) + \omega_n^2 q_n(t) = M_n^{-1} w_n^d(t) + b_n u(t), \quad n = 1, 2, \ldots, N_m, \tag{2}$$

where

$$b_n = M_n^{-1} \int_{S(x,\,y)} \phi_n(x, y) L_{xy}[\beta(x, y)]\, \mathrm{d}S(x, y) u(t), \tag{3}$$

where M_n is the modal mass, ω_n is the natural frequency, $w_n^d(t)$ is the generalized disturbance force, L_{xy} defines the differential operator associated with the actuator, and $\beta(x, y)$ defines the spatial aperture over which the transducer is applied. As such, the differential action of the actuator, and its dimension and position relative to the structure, clearly influences the resulting generalized force applied through the modal participation coefficient, b_n.

Similarly, an expression for the sensor output, $y(t)$, can be developed as a function of the response in generalized coordinates as detailed by Clark *et al.* [1]. Specifically

$$y(t) = \sum_{n=1}^{N_m} c_n q_n(t), \tag{4}$$

where

$$c_n = \int_{S(x,\,y)} \sigma(x, y) S_{xy}[\phi(x, y)]\, \mathrm{d}S(x, y). \tag{5}$$

S_{xy} defines the differential operator associated with the sensor, and $\sigma(x, y)$ defines the aperture over which the sensor is applied. As with the expression for the actuator, the differential operation and aperture of the sensor play a critical role in the contribution of each structural mode to the output as demonstrated by the modal participation coefficient, c_n. This path-dependent response from actuator to sensor resulting from the spatial filtering allows for loop-shaping by transducer selection/design.

A proportional damping term is also included in the model to bound the plate response on resonance by adding the term $2\zeta_s \omega_n \dot{q}_n(t)$ to the left-hand side of equation (2). For this work, the localized mass and stiffness of the distributed piezoelectric transducers are assumed negligible during optimum spatial compensator design, but are included, using the approaches presented by Hagood et al. [10], for controller design and results analysis.

A diagram of the plate structure is shown in Figure 1. Two distributed transducers are applied to the plate for control: an actuator is applied at placement (x_a, y_a) and a sensor is applied at placement (x_s, y_s). The transducer sizes and placements shown in Figure 1 are arbitrary; the optimum transducer sizes and placements are to be selected with the design metrics discussed below. The physical dimensions and material properties of the plate are given in section 3.

For this work, it is assumed that the plate structure is driven by a *generalized disturbance*, $w_n^d(t)$, such that each plate mode is excited at the same input level with uncorrelated random noise, weighted by its modal mass. Each modal disturbance signal is assumed to be uncorrelated and have a unity power spectrum, i.e. $S_{w_n^d w_n^d}(\omega) = 1$. This form of plate excitation omits the spatial filtering effects of a specific disturbance transducer type, size, or placement. Thus, the resulting design and performance results are more applicable to a general variety of disturbance scenarios. For all examples provided in this manuscript, this

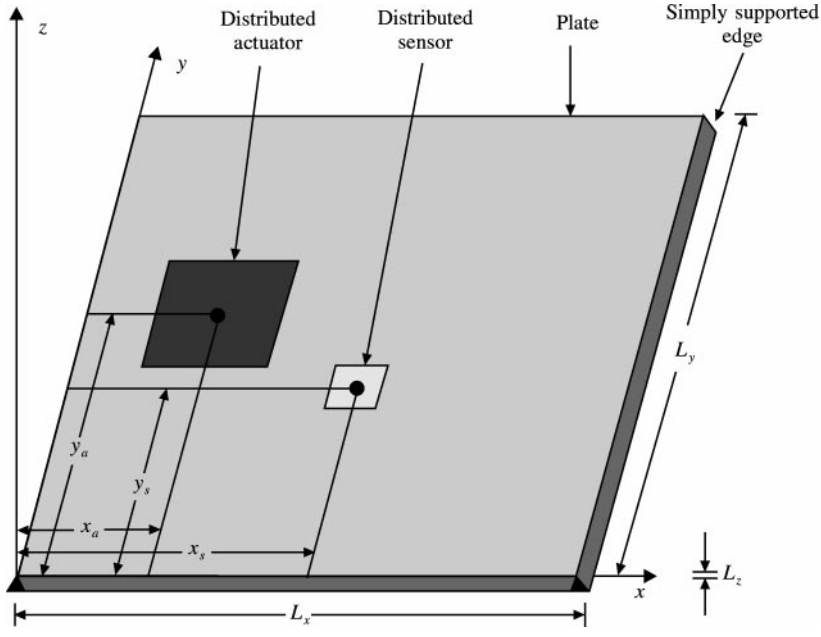

Figure 1. Diagram of simply supported plate (arbitrary transducers size and placement).

general form of disturbance will be applied, both for open-loop transducer selection and for closed-loop design of compensators.

2.2. DESIGN METRIC

The metric for optimum spatial compensator design presented here is developed from the work of Smith and Clark [8], Clark and Cox [7], Lim [9], Lim and Gawronski [11], and Gawronski and Lim [12]. These works detail a design technique that determines optimum transducer size and placement by maximizing a metric formed of approximate Hankel singular values of the open-loop controllability and observability Gramians [13]. The design metric presented here provides a balance between the selection of individual modes for coupling and de-coupling, and is necessary when one considers a range of transducer sizes.

The spatial width and length (size) of a distributed transducer have a significant influence on the magnitude of the coupling with the structure. This coupling gain level can vary by many orders-of-magnitude over a relatively small range of transducer sizes, and influences how the optimum spatial compensator design metric must be formulated. Previous work by Clark and Cox [7] considered a fixed transducer size, and thus the optimum results were not affected by variation in coupling gain level.

The first step in developing any compensator design metric is to cast the control problem into proper form. Figure 2 shows a block diagram of the two-port or two-input, two-output (TITO) closed-loop system. The system $T(s)$ is composed of the generalized plant, $P(s)$, with controller, $K(s)$. The transfer matrix $P(s)$ in Figure 2 represents the dynamics of the simply supported plate and transducer coupling. In addition, when $P(s)$ is used to formulate the spatial and temporal compensator design problems, it also includes the appropriate weighting functions as desired for sensor noise inputs and/or performance outputs [1].

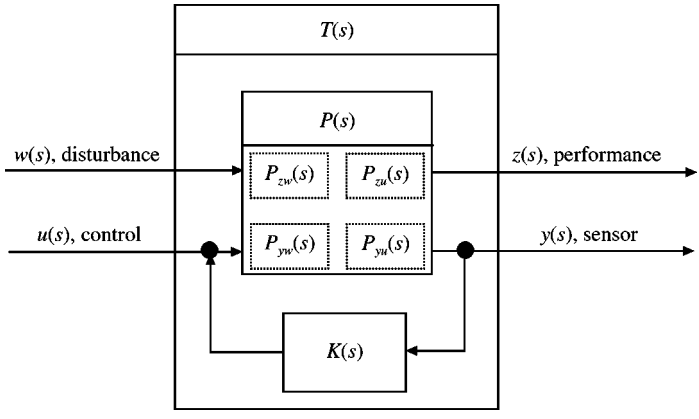

Figure 2. Block diagram of generalized plant with feedback controller.

Four transfer matrices can be identified through the standard generalized plant format. The upper-left transfer matrix, P_{zw}, represents the path from the input disturbance signals to the desired performance. The lower-right transfer matrix, P_{yu}, is the path from the input actuator signal to the measured sensor output, and is determined by the selection of transducer type, size, and placement as shown in equations (3) and (5). The cross-transfer matrices P_{zu} and P_{yw} show that the control transducers also affect system performance and that the disturbance signals affect the measured outputs respectively. As shown in references [7, 8], and further demonstrated in this work, one can influence the coupling to selected modes and crudely loop-shape the adaptive structure.

The optimum transducer properties are determined by maximizing a metric formed from the proper transfer matrices. For lightly damped structures, the value of each HSV of a transfer matrix is associated with a state of the system, and the size of each provides a relative measure of the contribution that the state makes to the input–output response.

For the development, cast the structural model from the actuator input, $u(t)$, to the measured output of the sensor, $y(t)$, in modal form such that

$$\ddot{\mathbf{q}} + \mathrm{diag}(2\zeta_i\omega_i)\dot{\mathbf{q}} + \mathrm{diag}(\omega_i^2)\,\mathbf{q} = \hat{\mathbf{B}}u, \quad y = \hat{\mathbf{C}}\mathbf{q}, \tag{6}$$

where ω_i and ζ_i are the natural frequency and damping ratio of the ith mode respectively. Defining the state vector as

$$\mathbf{x} = [\dot{q}_1, \omega_1 q_1, \ldots, \dot{q}_{N_m}, \omega_{N_m} q_{N_m}]^{\mathrm{T}} \tag{7}$$

produces a state-space representation such that

$$\dot{\mathbf{x}} = \mathbf{A}\mathbf{x} + \mathbf{B}\mathbf{u}, \qquad y = \mathbf{C}\mathbf{x}, \tag{8}$$

where $\mathbf{A} = \mathrm{diag}(\mathbf{A}_i)$, $\mathbf{B} = [\mathbf{B}_1^{\mathrm{T}}, \ldots, \mathbf{B}_{N_m}^{\mathrm{T}}]^{\mathrm{T}}$, $\mathbf{C} = [\mathbf{C}_1, \ldots, \mathbf{C}_{N_m}]$. The submatrices are defined as

$$\mathbf{A}_i = \begin{bmatrix} -2\zeta_i\omega_i & -\omega_i \\ \omega_i & 0 \end{bmatrix}, \qquad \mathbf{B}_i = \begin{bmatrix} \mathbf{b}_i^{\mathrm{T}} \\ \mathbf{0} \end{bmatrix} \tag{9, 10}$$

and

$$\mathbf{C}_j = [\mathbf{c}_j, \mathbf{0}] \tag{11}$$

where $\mathbf{b}_i^{\mathrm{T}}$ is the ith row of $\hat{\mathbf{B}}$ and $\mathbf{c}_j$ is the jth column of $\hat{\mathbf{C}}$ [13].

Williams [13] demonstrated that the square of the ith HSV of a lightly damped structure can be approximated by

$$\gamma_i^4 = \frac{[\mathbf{b}_i^{\mathrm{T}}\mathbf{b}_i]\,[\mathbf{c}_i^{\mathrm{T}}\mathbf{c}_i]}{(4\zeta_i\omega_i)^2}, \tag{12}$$

where γ_i^2 is the approximation of the ith HSV. As indicated in equation (12), the $i$the HSV is proportional to the time constant ($\tau_i = 1/(\zeta_i\omega_i)$) of the ith structural mode and the modal participation coefficients for each actuator and sensor. The numerator of equation (12) thus provides a measure of the degree of coupling between the actuator inputs and measured outputs relative to the structural modes. Physically, the HSV is a measure of the amount of energy that can be stored in the system from the inputs and the amount of energy that can be retrieved by the outputs [14]. Thus, the HSV can be used to measure the effectiveness of a particular actuator/sensor pair for coupling or not coupling to structural modes.

For the generalized plant given in Figure 2, the vector of HSVs of the open-loop system from the input actuator signal, u, to the sensor output, y, is written as

$$\Gamma_{yu}^2 = \mathrm{diag}(\gamma_{yu1}^2, \ldots, \gamma_{yun}^2, \ldots, \gamma_{yuN_m}^2). \tag{13}$$

A design metric based entirely upon evaluating equation (13) was first presented in references [11, 12]. In this case, each HSV was computed for a predetermined set of candidate transducer placements and the optimum placement is that which provided the greatest value. The conclusion of this work was that selecting transducer placements with the largest degree of coupling increases control system efficiency and, thus, overall performance.

Lim [9] recognized that the purpose of the control problem defined in Figure 2 is to reduce/control the system performance, $z(s)$, and to serve that purpose, equation (13) was weighted by a measure of the system performance to provide for spatial compensator designs that are efficient at coupling to the modes with the greatest effect on $z(s)$. This technique also allowed one to consider the influence of disturbance path on system performance. Lim [9] defined a measured of the degree of coupling of each mode associated with the performance disturbance path, P_{zw}:

$$\Gamma_{zw}^2 = \mathrm{diag}\,(\gamma_{zw1}^2, \ldots, \gamma_{zwn}^2, \ldots, \gamma_{zwN_m}^2). \tag{14}$$

An optimum spatial compensator design metric was then written as a function of the squares of the approximate HSVs:

$$J_{qp} = \sum_{n=1}^{N_m} \frac{\gamma_{y_p u_q n}^4}{\gamma_{yun}^4}\,\gamma_{zwn}^4, \tag{15}$$

where J_{qp} is the metric for the qth candidate sensor and the pth candidate actuator. The value γ_{yun}^4 is the square of the nth HSV of the system, where all possible actuators and sensors are considered; it is used to normalize the HSV calculations. As shown in reference [9], equation (15) is a computationally efficient means of determining transducer designs that increase system performance.

Based upon equation (15), Clark and Cox [7] developed a design metric which also provided for system robustness. This metric emphasized coupling to models within the bandwidth of control, but de-emphasized coupling to modes outside the performance bandwidth. As detailed in reference [1], feedback control problems are susceptible to stability issues due to poor model fidelity beyond the bandwidth of performance, and previous approaches to limit the participation of out-of-bandwidth modes included low-pass filter hardware and loop-shaping of the temporal compensator to provide

roll-off at some predetermined frequency. Model fidelity limitations are typically imposed by computational speed and memory size of the digital signal processor hardware. Through transducer optimization, Clark and Cox [7] limited the de-stabilizing effects of out-of-bandwidth modes naturally, thus increasing system robustness to unmodelled dynamics.

Clark and Cox [7] distinguished between the number of in-bandwidth modes, n_{in}, and the number of out-of-bandwidth modes, $n_{out} = N_m - n_{in}$, by forming the design metric as

$$\hat{J}_{qp} = \bar{J}^{in}_{qp} + \bar{J}^{out}_{qp}. \tag{16}$$

The cost for the in-bandwidth modes, $\bar{J}^{in}_{qp}$, was defined as equation (15) over the first n_{in} modes and normalized with respect to its maximum entry. The cost for the out-of-bandwidth modes was defined to emphasize poor coupling to those modes and is written as

$$J^{out}_{qp} = \left(\sum_{n=n_{in}+1}^{N_m} \frac{\gamma^2_{y_p u_q n}}{\gamma^4_{yun}} \gamma^4_{y_p u_q n} \right)^{-1}. \tag{17}$$

The term $\bar{J}^{out}_{qp}$ in equation (16) is defined as equation (17) divided by its maximum entry over the entire candidate set.

As shown by Clark and Cox [7], equation (16) resulted in an optimum spatial compensator design that efficiently coupled to modes at low frequencies and rolled off naturally at high frequencies. This method provided a simple type of loop-shaping by spatial design and increased the robustness of the adaptive structure by balancing in-bandwidth coupling to structural modes important for performance against the inherent out-of-bandwidth roll-off provided by the chosen transducer pair.

Smith and Clark [8] continued the advancement of spatial compensator design techniques by extending the design metric presented. Beyond considering in-bandwidth and out-of-bandwidth modes, Smith and Clark [8] presented a method to select modes for control and to de-emphasize modes, both in-bandwidth and out-of-bandwidth, not considered important by the control system designer. Limiting actuator-to-sensor coupling to only selected modes lowers the order of the modelled system, thus leading to lower order controllers. By definition, if a system does not observe/control modes, then they do not have to be modelled for temporal compensator design [15].

The coupling cost for the design metric of Smith and Clark [8] was written over all modes as

$$J^{ct}_{qp} = \sum_{n=1}^{N_m} \Lambda_n \frac{\gamma^2_{y_p u_q n}}{\gamma^4_{yun}} \gamma^4_{zwn}, \tag{18}$$

where Λ is a binary, selection vector of length N_m. Modes to be controlled have an element value of 1 in Λ. The de-coupling cost over all modes was written as

$$J^{nc}_{qp} = \left(\sum_{n=1}^{N_m} (\sim\Lambda)_i \frac{\gamma^4_{y_p u_q n}}{\gamma^4_{yun}} \gamma^4_{y_p u_q n} \right)^{-1}, \tag{19}$$

where the $\sim$ operator is the *one's compliment* or binary NOT. The design metric for mode selection, presented in reference [8], was written as

$$\tilde{J}_{qp} \equiv \bar{J}^{c}_{qp} + \alpha \bar{J}^{nc}_{qp}. \tag{20}$$

Again, the single overbar indicates that the individual metrics have been normalized by their maximum value before summation. The weighting α provides for a design tradeoff where $\alpha \geqslant 0$. A large value of α is selected for designs that de-emphasize coupling to the

modes not important for performance, and a small value of α is selected to emphasize coupling to the modes to be controlled. A typical choice for α is unity, but the parameter can be adjusted by the control system designer to modify the relative weighting.

The design metrics given by equations (16) and (20) normalize the individual cost terms associated with in-bandwidth coupling ad out-of-bandwidth roll-off before summation. However, as will be demonstrated by example in section 4.1, the application of the design metrics is limited to problems whereby the dimensions of the actuators and sensors are fixed (i.e., where placement is the only design variable). This limitation results because the signal gain of a given type of transducer diminishes as the size of that transducer diminishes, approaching zero in the limit. As such, the portion of the performance metric aimed at minimizing coupling to modes beyond the bandwidth of control naturally decreases as the transducer dimension gets smaller. This "feature" serves to emphasize the selection of transducers with "small" dimensions to minimize coupling to structural modes at high frequency. In contrast, if the application of the design metrics presented in equations (16) and (20) is limited to cases whereby placement is the only design issue (i.e., fixed transducer size), then a reduction in modal coupling is a direct result of wavenumber filtering as opposed to signal gain based upon transducer size. As such, the design metrics given by equations (16) and (20) are only practical when the dimensions of the actuators and sensors are fixed, but the positions of the transducers on the structure are allowed to vary.

To provide for a balance between coupling and de-coupling when the candidate set has varying transducer sizes and thus coupling gain levels, the two cost terms should be multiplied and then normalized, which is the specific focus of this paper. The design metric is written as

$$\tilde{\tilde{J}}_{qp} \equiv \overline{(J^c_{qp} J^{nc}_{qp})}. \tag{21}$$

Transducers with a small coupling gain level will produce a large value for J^{nc}_{qp} (see equation (19)). However, they will also produce a small value for J^c_{qp} and, when the two costs are multiplied, a small metric results. Transducers with large coupling gain levels will produce a large J^c_{qp}, but a small J^{nc}_{qp} cost. Large values of equation (21) are only given when both J^c_{qp} and J^{nc}_{qp} are large in value. This results when both the transducer size and placement are optimum for the desired modal selection. Section 4.1 also gives a direct comparison of optimum spatial compensator designs using equations (20) and (21).

2.3. $\mathscr{H}_2$ CONTROL

The $\mathscr{H}_2$ controller design process involves the minimization of the $\mathscr{H}_2$ norm of closed-loop transfer matrix, T_{zw}, by the specification of a proper $K(s)$. The $\mathscr{H}_2$ controller design problem is solved here using the state-space solutions presented in reference [16]. This process involves solving two Riccatti equations by Schur decomposition and realizes a full dynamic compensator, $K(s)$, that is unique and of dimension equal to that of $P(s)$ [15]. The solution is also stable, proper and, hence, realizable.

Since the dimension of the compensator, $K(s)$, is equal to that of the plant model, $P(s)$, used in the design, reducing the order of adaptive structure model by de-emphasizing coupling to all modes considered unimportant for performance leads to a lower-order compensator. The actuator and sensor serve as wavenumber filters and if they can be designed concurrently to limit coupling to only those modes present in the performance path, then the order of the resulting compensator is also constrained to the order of that minimal dynamic representation.

3. PHYSICAL SYSTEM

The geometry of the physical system is shown in Figure 1. The plate physical dimensions and material properties are provided in Table 1. The thickness and properties of the distributed piezoelectric transducers are provided in Table 2. The values given in Tables 1 and 2 are assumed fixed. The mass and stiffness effects of the distributed piezoelectric transducers are minimized by specifying a patch thickness that is significantly less than the plate thickness. They are only included in the model when designing the $\mathscr{H}_2$ controllers and analyzing the closed-loop results.

The open-loop design metric presented in equation (21) is used here to optimize the size and placement of distributed piezoelectric transducers for a plate structure. The design approach outlined provides a computationally efficient method of selecting the best actuator–sensor pair for the desired spatial filtering from a predetermined set of candidate actuators and sensors. For this work, a set of 1523^2 possible actuator–sensor configurations of varying size and placement is considered. To form the candidate set, the x- and y-dimensions of the distributed transducers are varied from 0·0508 m (2 in.) to 0·1524 m (6 in.), in steps of 0·0254 m (1 in.). The placement of each candidate transducer is then varied across the plate, from edge to edge, in steps of $0{\cdot}1 \times L_x$ and $0{\cdot}1 \times L_y$. This produce 3027 potential transducer sizes and placements, of which 1523 lie completely within the plate boundaries and are kept as the candidate set. In this development, all patches are assumed aligned with the coordinates of the plate.

A pair of 0·0508 m (2 in.) square transducers, colocated, with center placement at (0·2742, 0·0894) m, is selected as an initial, or non-optimal, case. This transducer size and placement was utilized in previous studies on control of plate structures with distributed transducers [17], and will be compared with the optimum design results.

TABLE 1

Properties of plate structure

Property	Value
Material	Aluminum
Width, L_x	0·4572 m
Height, L_y	0·4064 m
Thickness, L_z	0·0048 m
Density, ρ_s	2700 kg/m^3
Young's modulus, E_s	$7{\cdot}1 \times 10^{10}$ N/m^2
Poisson's ratio, ν_s	0·33
Damping ratio, ζ_s	0·02

TABLE 2

Properties of distributed piezoelectric transducers

Property	Value
Material	G-1195 PZT
Thickness, L_z^p	0·0002 m
Density, ρ_p	7650 kg/m^3
Young's modulus in E_{11}, E_p	$4{\cdot}9 \times 10^{10}$ N/m^2
Poisson's ratio, ν_p	0·30
Strain coefficient, d_{31}	-166×10^{-12} m/V

The analytical plate model is calculated over the first 75 plate modes ($N_m = 75$) and is thus accurate to approximately 5 kHz. However, the bandwidth of interest for the control results is selected between 10 and 2000 Hz, which includes 19 structural modes (i.e., 38 states). For the open-loop actuator and sensor design/selection problem, the disturbance input vector, $\mathbf{w}(s)$ (illustrated in Figure 2), is composed of process noise, represented by $\mathbf{w}_d(s)$. The vector is of dimensions $N_m \times 1$ and represents uncorrelated random noise applied to each structural mode (i.e., $\mathbf{w}(s) = \mathbf{w}_d(s)$). For the closed-loop design of the dynamic compensator, an additional input, $w_s(s)$, is added to the disturbance input vector, $\mathbf{w}(s)$, to represent sensor noise such that $\mathbf{w}(s) = [\mathbf{w}_d^{\mathrm{T}}(s)\ w_s(s)]^{\mathrm{T}}$. The modal velocities of the structural modes targeted for control, with modal indices of (1,1), (3,1), (1,3), and (3,3) for the example provided, are used to define the performance vector, $z(s)$, for all open-loop actuator/sensor designs and for the closed-loop design examples. The actuator and sensor inputs and outputs, respectively, are represented by $u(s)$ and $y(s)$ and correspond physically to piezoelectric transducer pairs from the original candidate sets.

4. RESULTS AND DISCUSSION

The adaptive structure design problem for this work is to reduce, with a single sensor and actuator transducer pair, the vibration response of the (1,1), (1,3), (3,1) and (3,3) modes of a simply supported plate. These four modes are the plate's most efficient acoustic radiators [1, 2]. To add robustness with respect to unmodelled dynamics and limit controller order, it is also desirable to minimize coupling to the other plate modes.

The first ten damped natural frequencies of the plate are given in Table 3, where the selection vector for this design problem is shown in the last column. The four modes which are chosen as important for control have a Λ value of 1. Other modes within the design bandwidth have a Λ value of 0, indicating that they are not important for control and the spatial compensation resulting from the optimum transducer pair should, ideally, not couple to them. To also ensure high-frequency roll-off, all modes above (3,3) have a selection value of 0, i.e., $\Lambda_{11\ldots N_m} = 0$.

The optimum transducer size and placement that meets the design goals of maximizing coupling to the four most efficient plate radiators and minimizing coupling to all other modes is not immediately obvious to the control system designer. Thus, the design methods presented in section 2.2. must be utilized.

TABLE 3

Plate modes, damped natural frequencies and selection vector

Mode number, n	Mode index, (n_x, n_y)	ω_d (Hz)	Λ_n
1	(1,1)	127	1
2	(2,1)	295	0
3	(1,2)	340	0
4	(2,2)	510	0
5	(3,1)	577	1
6	(1,3)	697	1
7	(3,2)	789	0
8	(2,3)	864	0
9	(4,1)	969	0
10	(3,3)	1144	1

Before presenting the optimum spatial compensator design results for this problem, a comparison of the design metrics of equations (20) and (21) is given in section 4.1. The benefits of a product metric over a summed metric are demonstrated by means of a reduced candidate set example. The optimum transducer size and placement determined from the full candidate set are then presented in section 4.2.1. The coupling between the actuator input and sensor output for both the initial and optimum designs is compared. These results demonstrate that the optimum design balances the design goals of coupling to the selected modes and minimizing coupling to all other modes. The motivation for this work is to demonstrate that spatial compensator design influences the controller design and the resulting adaptive structure performance and robustness to unmodelled dynamics. The controller design approach for this work is presented in section 4.2.2. To ensure proper comparison of closed-loop results for different transducer pairs, the control effort weighting and sensor noise gains were adjusted such that the controller utilized the same level of signal energy for both the initial and optimum spatial compensator designs. The loop gain and closed-loop performance of each design are then presented in sections 4.2.3 and 4.2.4 respectively. These results are discussed in terms of the control objectives of performance and selected coupling.

4.1. COMPARISON OF DESIGN METRICS

The design metrics of equations (20) and (21) are compared and discussed in this section. A reduced candidate set is considered to allow for plotting of the design metrics and is formed by assuming a dimension site size of 0·0508 m (2 in.), instead of 0·0254 m (1 in.), and a placement step size of $0{\cdot}25L_x$ and $0{\cdot}25L_y$, instead of 0·1. This gives a candidate set of 28 potential transducer sizes and placements over the plate, including the initial design. The exact size and placement of the initial transducer is given in the first row of Table 4.

Bar-charts of the design metrics for the reduced candidate set are given in Figure 3. Due to space limitations, the x- and y-axis labels are only shown on the upper left figure. The first set of results, Figure 3(a), shows the coupling cost $\bar{J}^c_{qp}$ (equation (18)) normalized by its maximum value. As expected, larger transducers give a higher cost value, due to increased

TABLE 4

Sensor and actuator size and placement for each design

Transducer	Center, (x, y) m	Width, Δx m	Height, Δy m
Initial			
Actuator	(0·2743, 0·0894)	0·0508	0·0508
Sensor	(0·2743, 0·0894)	0·0508	0·0508
Optimum ($\tilde{J}_{qp}$), *equation* (20) *with reduced candidate set*			
Actuator	(0·2286, 0·2032)	0·1524	0·1524
Sensor	(0·2286, 0·2032)	0·1524	0·1524
Optimum ($\tilde{\tilde{J}}_{qp}$), *equation* (21) *with reduced candidate set*			
Actuator	(0·2286, 0·1016)	0·1524	0·1524
Sensor	(0·1143, 0·2032)	0·1524	0·1524
Optimum ($\tilde{\tilde{J}}_{qp}$), *equation* (21)			
Actuator	(0·0914, 0·0813)	0·1016	0·1016
Sensor	(0·2286, 0·2032)	0·1270	0·1270

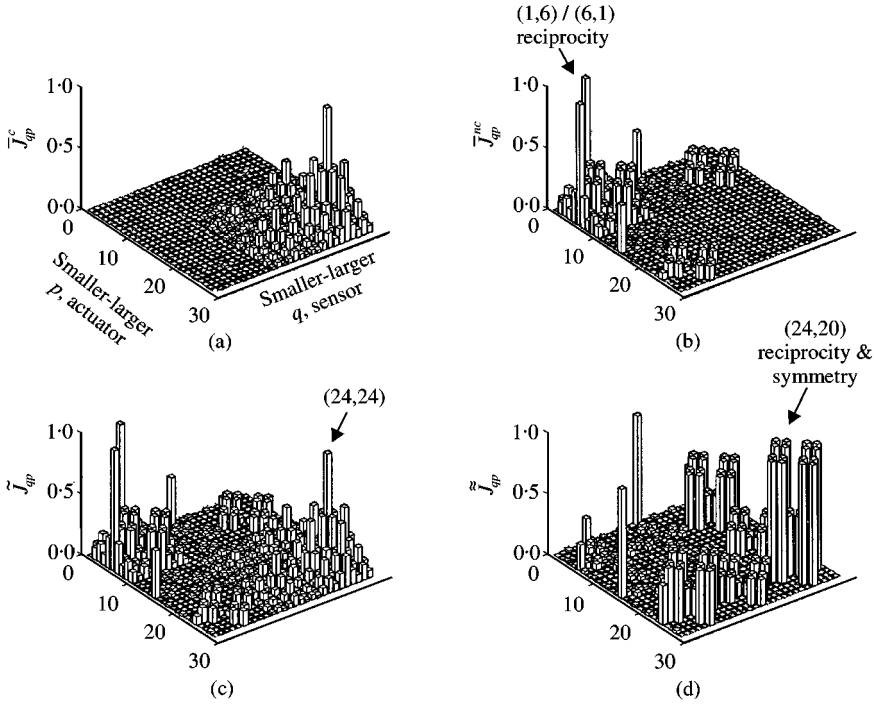

Figure 3. Bar-chart of design cost and metrics for each transducer combination in the reduced candidate set: (a) coupling cost $\bar{J}^c_{qp}$ (equation (18)); (b) de-coupling cost $\bar{J}^{nc}_{qp}$ (equation (19)); (c) coupling cost $\tilde{J}_{qp}$ (equation (20)); (d) coupling cost $\tilde{J}_{qp}$ (equation (21)).

coupling to the larger spatial waves of the (1,1), (1,3), (3,1) and (3,3) modes defining the performance metric. The maximum value in this case is given by the largest patch pair (6 in.), colocated at the center of the plate; this is the optimum positioning for coupling to odd structural modes.

Figure 3(b) shows a bar-chart of the de-coupling cost $\bar{J}^{nc}_{qp}$, equation (19) normalized by its maximum value. Here the smaller transducers give the higher cost because they have the lowest coupling gain level. The effect of the decrease in coupling gain level with smaller transducers is greater than the spatial filtering effect of the larger aperture transducers (further discussion on this point is given below). Also, note that the results in Figure 3(b) show the reciprocity of the linear plate structure; the cost for actuator 6 and sensor 1 has the same value as for sensor 6 and actuator 1.

The design metric of Smith and Clark [8], equation (20), is given in Figure 3(c) for $\alpha = 1$. The costs of Figure 3(a) and 3(b) sum together to form a chart with three maximum peaks. The peak at actuator 24 and sensor 24 is chosen by the numerical routine as optimum; the transducer size and placement of this design is given in the second row of Table 4. Adjusting the value of α for this case would force the choice of one optimum over the other. No balance between coupling and de-coupling results from the application of equation (20) when transducer sizes are allowed to vary.

Figure 3(d) is a bar-chart of the design metric formed by multiplying unnormalized versions of Figure 3(a) and 3(b), equation (21). A cluster of transducer combinations give maximum value. Due to reciprocity and plate symmetry, the peaks all correspond to the same spatial compensator; each of the small clusters is a result of the same actuator and sensor placements in different quadrants of the plate. The optimum design is selected from

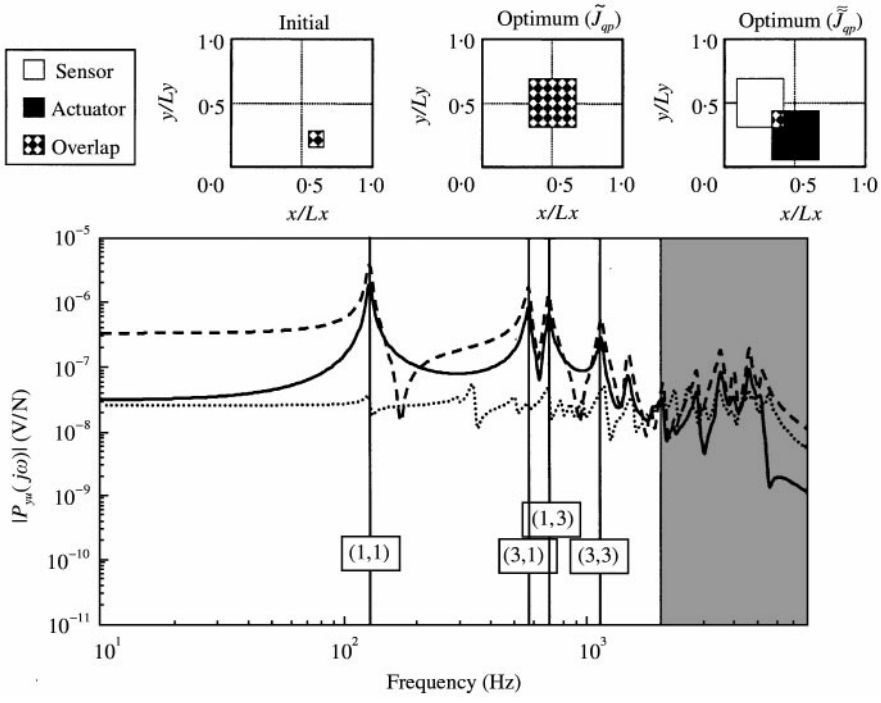

Figure 4. Sensor and actuator size and placement (normalized dimensions) for initial and optimum (with reduced candidate set) designs and magnitude of the frequency response of the actuator-to-sensor transfer functions: ·····, initial actuator/sensor; -----, optimal actuator/sensor based upon $\tilde{J}_{qp}$ (equation (20); ——, optimal actuator/sensor based upon $\tilde{\tilde{J}}_{qp}$ (equation (21)).

this set and given in the third row of Table 4. This result corresponds to a spatial compensator design that was not previously apparent in the individual costs (see Figure 3(a) and 3(b)) and, as shown below, represents a design that more appropriately balances both modal coupling and de-coupling.

Figure 4 gives the sensor and actuator size and placement for the three design cases: initial, optimum based upon equation (20) ($\tilde{J}_{qp}$), and optimum based upon equation (21) ($\tilde{\tilde{J}}_{qp}$). Results for the optimum based upon equation (21) ($\tilde{\tilde{J}}_{qp}$) are an actuator and sensor pair placed on mid-lines of the plate, with a slight overlap.

The magnitude of the frequency response of the transfer function P_{yu} is also shown in Figure 4. These curves represent the actuator-to-sensor coupling for each design. The input signal to each actuator is the prescribed voltage and the sensed output is the piezoelectric charge, which is proportional to structural strain. Vertical lines have been drawn in Figure 4 at the frequencies of the desired modes to control; each line is labeled with the corresponding modal index. The shaded portion of Figure 4 represents the frequency area outside the design bandwidth.

The actuator-to-sensor frequency response function for the initial design is immediately recognizable in Figure 4. Due to the colocated positioning and small size, the frequency response is characterized by an alternating set of poles and zeros, and has a relatively small coupling gain level that is roughly constant in magnitude. The optimum based upon equation (20) ($\tilde{J}_{qp}$) is also colocated, and has a transducer frequency response characterized by an alternating set of poles and zeros. However, the gain level for this case is much higher due to the center placement and larger aperature. The coupling gain also begins to decrease

at high frequency due to spatial filtering effects of the larger transducer size. These results are consistent with the work of Vipperman and Clark [17], which showed that colocated transducers with large aperatures provided greater control of low-bandwidth modes and serve as spatial wavenumber filters of higher modes. This is also an "intuitive" spatial design from observing nodal lines.

The actuator-to-sensor frequency response for the optimum based upon equation (21) ($\tilde{\tilde{J}}_{qp}$) shows slightly less coupling to the desired modes than the optimum based upon equation (20) ($\tilde{J}_{qp}$), but also shows less coupling to the modes de-emphasized for control. This solution represents a balance between the design goals and demonstrates the usefulness of the metric given by equation (21), demonstrating the ability to design spatial compensators that shape the system frequency response through the control path.

4.2. OPTIMUM DESIGN RESULTS

Given that the advantages of applying the performance metric of equation (21) were demonstrated in section 4.1, it is now applied to the full candidate set (1523^2 transducers) and the optimum spatial compensator design results are obtained. The actuator-to-sensor coupling, loop gain, and closed-loop performance of the optimum design and the initial design are compared and discussed in this section. To ensure that the comparison of the closed-loop design and results is appropriate, the sensor noise gain is set relative to the frequency response between the applied process noise and the measured output, and the broadband control signal energy level of each design is normalized by adjusting the control effort weighting during $\mathscr{H}_2$ controller synthesis [18].

4.2.1. *Optimum spatial compensator*

The sensor and actuator size and placement, from the full candidate set, that maximize the value of $\tilde{\tilde{J}}_{qp}$ are given in the bottom row of Table 4 and plotted in Figure 5. The optimum design for this case is a large sensor positioned on the center of the plate and a slightly smaller actuator positioned in the lower left-hand corner. Unlike the previous results given by the reduced candidate set, the optimum design does not utilize the largest possible transducer. As also shown in Figure 5, the magnitude of the frequency response from the actuator to sensor for this optimum design only couples well to the four targeted modes. There is considerably less coupling to the non-targeted modes than in the previous results (compare with Figure 4).

As discussed in section 2.2, the optimum spatial compensator design metric decreases the sensitivity of the modelled adaptive structure to out-of-bandwidth modes by choosing a transducer size and placement that frequency-shapes the P_{yu} transfer function appropriately. The optimum design shows both high-frequency roll-off and de-coupling from modes not considered important for control, i.e., excluded from the selection vector, Λ.

Figures 4 and 5 show the influence that the open-loop design metric has on the actuator-to-sensor frequency response function of the adaptive structure. Through the cross-transfer matrices, P_{zu} and P_{yw}, spatial compensator design also affects the controller design and thus system loop gain and performance. Results and analysis of this influence are presented after a discussion of the controller design process.

4.2.2. *$\mathscr{H}_2$ Controller design*

Before discussing how the spatial compensator design influences the system loop gain and performance, it is important to detail how the $\mathscr{H}_2$ controller was developed. Controllers

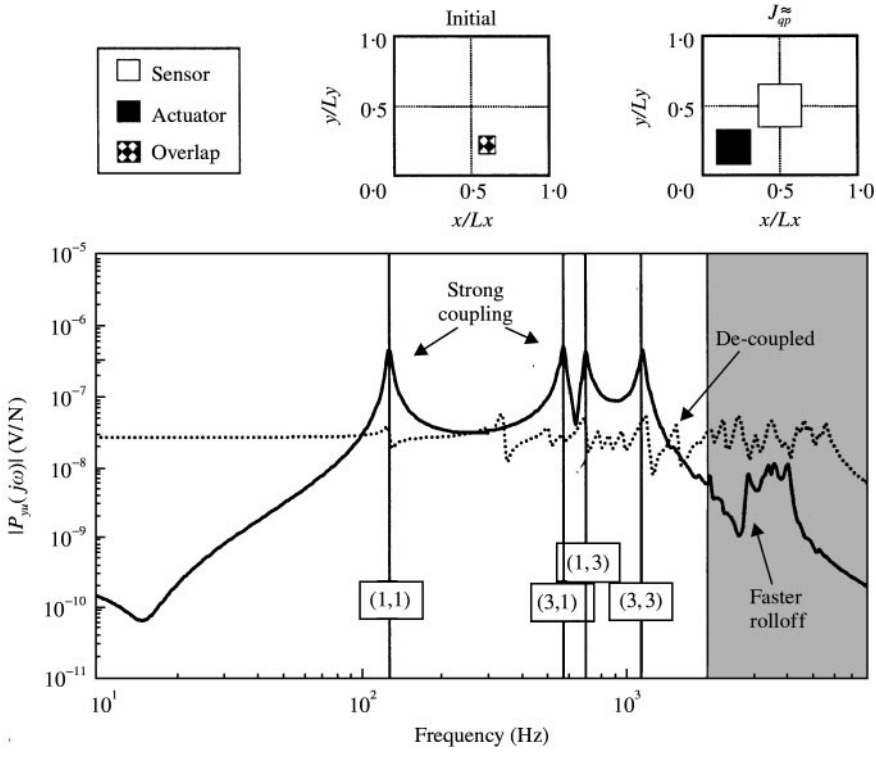

Figure 5. Sensor and actuator size and placement for initial and optimum designs (normalized dimensions) and magnitude of the frequency response of the actuator-to-sensor transfer functions: ·····, initial actuator/sensor; ——, optimal actuator/sensor based upon $\tilde{J}_{qp}$ (equation (21)).

are designed from models of the adaptive structures, whether analytical or experimental. In experimental work, system identification techniques are used to obtain accurate models over the performance bandwidth. To accurately capture this process, the $\mathscr{H}_2$ controllers in this work are designed with a model of the plate structure that only includes 19 plate modes (i.e., 38 states). This represents a system model that captures plate dynamics up to 2000 Hz and omits the inclusion of modes at higher bandwidth. Therefore, the non-shaded portion in Figures 4 and 5 represents both the limit of the performance bandwidth and the limit of the model bandwidth for controller design. It should be noted here that through careful selection of the actuator and sensor path, it may be possible to significantly reduce the order of the model from 38 states to approximately 8 states, if coupling is sufficiently limited to the (1,1), (3,1), (1,3), and (3,3) modes.

The $\mathscr{H}_2$ controller design process assumes a level of random measurement noise on each sensor signal and a unity process noise applied to each structural mode. The sensor noise signal is an uncorrelated zero-mean Gaussian process with a shaped spectral density. A comparison of the sensor output due to unit norm noise and unit norm disturbance signals applied to each structural mode is given in Figure 6 for the both the initial and optimum spatial compensator designs (i.e., for the two alternative transducer pairs considered in the design). The reduced system model (19-mode model) is being utilized during this portion of the controller design process.

For both designs, the sensor noise curve is created by a transfer function with three poles at 0·01 Hz and three zeros at 200 Hz. The sensor noise curve has high gain at low frequency to reduce control spillover below the first structural mode. The sensor noise gain for each

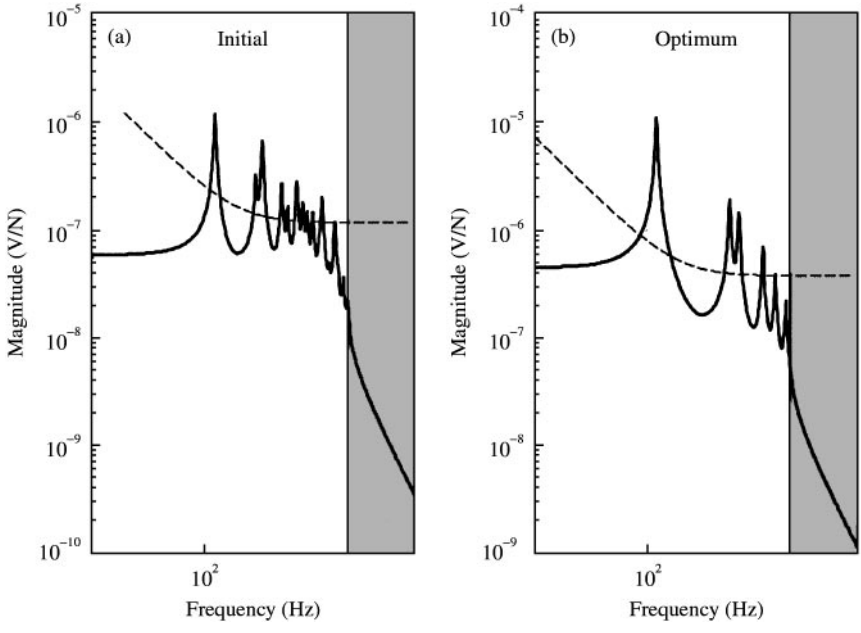

Figure 6. Sensor noise for each design case (reduced plate model): (a) magnitude of frequency response for initial actuator/sensor; (b) magnitude of frequency response for optimal actuator/sensor $\tilde{\tilde{J}}_{qp}$ (equation (21)) ——, Process noise $\| P_{yw_d}(j\omega)|$; ------, sensor noise $\| P_{yw_s}(j\omega)|$.

TABLE 5

Sensor noise gain, control effort weighting, resulting control power for each design

Design case	V_s	R_c	$\| T_{uw} \|_2$ (V/N)
Initial	$2{\cdot}3 \times 10^{-3}$	$4{\cdot}0 \times 10^{-4}$	149·198
Optimum	$7{\cdot}5 \times 10^{-3}$	$4{\cdot}301 \times 10^{-4}$	149·193

design case illustrated in Figure 6(a) and 6(b), respectively, is selected such that the contribution of the sensor noise is greater than the contribution of the process noise at the measured output of the system for frequencies beyond the design bandwidth. The gain associated with the sensor noise for both spatial compensator designs is given in Table 5 as V_s. The value of V_s is greater for the transducer pair resulting from the optimal, open-loop, design because the output response of the sensor is greater for the same level of applied process noise. A significant effort was made to ensure that the sensor noise curves for each design were applied consistently for the $\mathscr{H}_2$ controller designs. Obviously, there is a level of subjectivity here because different sensors are being used in each case. However, the objective is to design a compensator that minimizes the response of the (1,1), (3,1), (1,3), and (3,3) structural modes and also minimizes coupling to all other modes, particularly those at high frequency in interest of reducing the sensitivity of the system to unmodelled dynamics beyond the bandwidth of interest.

To further ensure proper comparison of results, the control effort weighting for the optimum spatial compensator design was adjusted such that the controllers resulting from each design case utilized the same amount of control signal energy as the initial case.

Control signal energy is defined as the $\mathscr{H}_2$ norm of the disturbance-to-control signal closed-loop transfer matrix, T_{uw}, over the modal bandwidth. The control effort weighting, designated by R_c, and the control signal energy levels for both designs are provided in Table 5.

4.2.3. *Comparison of loop gain*

One approach to optimum compensator design is to frequency-shape the *loop gain* of the adaptive structure [1, 15]. Loop gain is defined as the magnitude of the open-loop transfer matrix $P_{yu}K$, where the input is the control input and the output is that of the compensator. It is desirable to have a high loop gain at low frequency, where the disturbance dominates the structural response and the plant is well modelled. The loop gain should also be small at high frequency to reduce the effect of noise and avoid stability issues. At high frequencies, the noise signals can dominate the sensor response and, as discussed previously, the plant dynamics are, at best, poorly modelled. The exact cross-over point between high and low frequency for this work is directly after the (3,3) mode or 1144 Hz. As such, the selection vector was chosen such that $\Lambda = 0$ for all modes above this point.

Figure 7 shows the magnitude and phase of the loop gain as a function of frequency for both the initial transducer pair and the optimal transducer pair. The high-frequency results show that both designs provide loop gain magnitudes that decrease with frequency. However, as desired, the loop gain associated with the optimal transducer pair set falls much more sharply with frequency outside the model bandwidth. Thus, the loop gain has been shaped for desired characteristics simply by use of the optimum spatial compensator design (transducer sizes and placements). In fact, the order of the compensator can be significantly reduced for this case. As illustrated in Figure 7, the loop gain associated with the optimal transducer pair is dominated by four structure modes, corresponding to eight states of the model. As such, the resulting compensator focuses most of the control energy

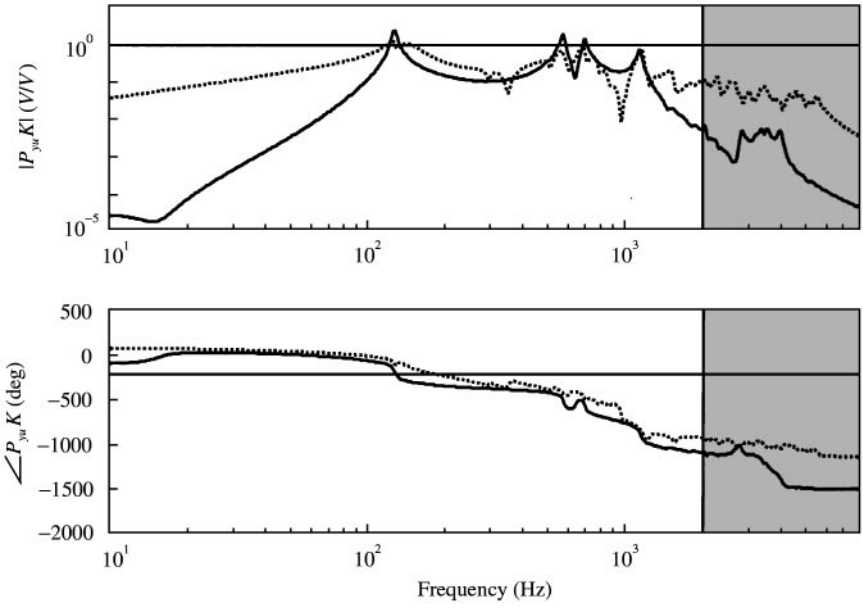

Figure 7. Loop gain for (·····) initial and (——) optimum designs (equal controller energy and similar sensor noise curves).

on those four structural modes. Model reduction can thus be applied with little degradation in closed-loop performance. This is a significant advantage for experimental systems as it provides a means of implementing a low-order compensator which would not otherwise be possible if the transducer pair were not designed to minimize coupling to modes not present in the chosen performance metric. Low-order compensators, from a practical perspective, are much easier to implement in current hardware.

4.2.4. *Comparison of Performance*

The vibration control performance corresponding to the H_2 norm of the modal velocities associated with the (1,1), (3,1), (1,3), and (3,3) modes for a unit norm disturbance input is provided as a function of frequency for each design in Figure 8. The open-loop performance of the system ($\| P_{zw_d}(j\omega) \|_2$) is provided as a reference against which the closed-loop performance ($\| T_{zw_d}(j\omega) \|_2$) can be evaluated where $\| \cdot \|_2$ is the $\mathscr{H}_2$ norm of the system at each frequency. For the open-loop case, the transducers are attached (i.e., incorporating the local mass and stiffness effects with initial size and placement) but not activated. The two lower curves show the closed-loop vibration performance, $\| T_{zw_d}(j\omega) \|_2$, when each control system has been activated. The results presented in Figure 8 are shown for a frequency resolution of 1 Hz. The units of performance are structural velocity per unit of input force.

The active insertion loss (AIL) in one-third-octave bands of each design is also given in Figure 8. Active insertion loss is defined as the reduction of performance by the activation of the control system [19]. It is characterized as $AIL \equiv 20 \log_{20} (\| P_{zw_d} \|_2 / \| T_{zw_d} \|_2)$. In this case, the term $\| T_{zw_d} \|_2$ is the $\mathscr{H}_2$ norm of the closed-loop disturbance-to-performance transfer matrix over one-third octave frequency bands and $\| P_{zw_d} \|_2$ is the $\mathscr{H}_2$ norm of the open-loop performance transfer matrix over the same bands. The units of AIL are decibels and positive values correspond to a reduction in vibration response associated with the modes included in the performance metric. The AIL ordinate is shown on the right-hand side of the figure and the one-third octave band center frequencies of selected bands are shown directly below the bands.

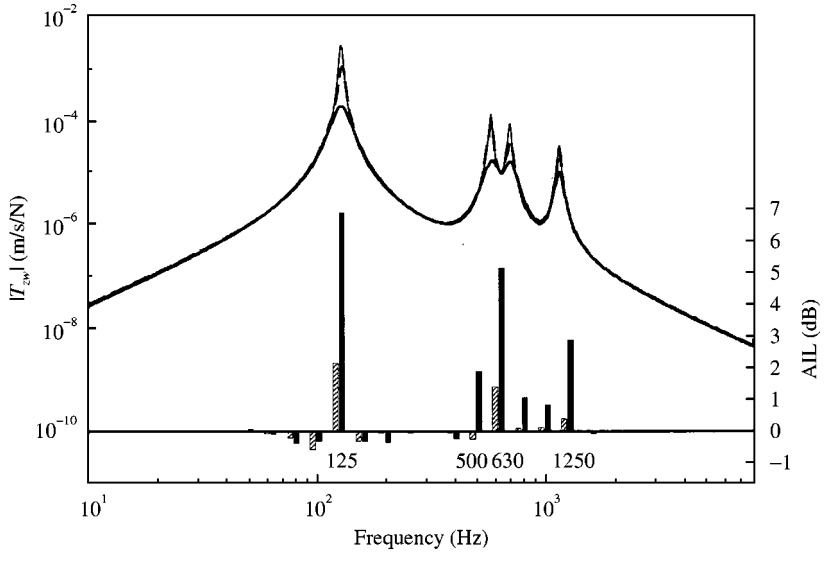

Figure 8. Vibration control performance and active insertion loss for each design case (equal controller energy and similar sensor noise curves): ——, open loop; ------, initial actuator/sensor; ——, optimal actuator/sensor.

TABLE 6

AIL, in selected one-third octave bands, for initial and optimum design

	AIL (dB)			
	One-third-octave band			
Design case	125 Hz	500 Hz	630 Hz	1250 Hz
Intitial	2·1	− 0·3	1·4	0·4
Optimum	6·9	1·9	5·1	2·9

The results given in Figure 8 show that the closed-loop performance resulting from the application of the initial transducer pair has a very limited effect on the plate response of the (3,1) and (3,3) modes. The closed-loop performance resulting from application of the optimal transducer pair is capable of controlling these modes and is much more effective at controlling at (1,1) and (1,3) modes, as expected, for the same level of control signal energy. AIL results for the one-third octave bands that include a selected mode are detailed in Table 4. These results show that the optimum design provides much greater control of the plate vibration for the targeted modes. Control of all the selected modes is more than tripled between the initial and optimum spatial compensator designs, while both controllers are using the same amount of control signal energy. By altering the size and placement of the transducers used for control, the performance of the adaptive structure has been greatly increased.

5. CONCLUSIONS

The development of a computationally efficient and proper manner to pose the optimal design of actuators and sensors to provide loop-shaping through adaptive structure design is the primary contribution of this paper. Since the Hankel singular values of a lightly damped structure can be estimated in a computationally efficient manner, the optimal actuator and sensor for producing a desired loop shape can be determined by minimizing a cost function that emphasizes the coupling to modes important for performance and penalizes coupling to all other modes within and beyond the bandwidth of interest.

To demonstrate the design concept, an example was provided. A single piezoelectric actuator and sensor were designed for a plate with pinned boundary conditions. A performance metric was chosen to limit coupling to the (1,1), (3,1), (1,3), and (3,3) modes of the structure. The frequency response of the resulting actuator–sensor pair limited coupling almost exclusively to the modes targeted in the performance metric. In the design of adaptive structures, if spatial compensation (i.e, loop-shaping) can be incorporated into the design, low-order models of the structure can be used for control system implementation. If the path-dependent frequency response of the structure is dominated by modes that must be controlled to achieve the desired level of closed-loop performance, then the model resulting from system identification on the physical structure will contain fewer states and will thus lead to low-order dynamic compensators, whether they be adaptive or fixed gain. Based upon these observations, it is concluded that emphasis should be placed on designing spatial compensators in order to facilitate the design of controllers for adaptive structures. Through proper design and planning, the implementation of a controller can be greatly simplified, which in the authors' opinion is a critical feature of an adaptive structure.

ACKNOWLEDGMENTS

The authors gratefully acknowledge that this work was supported in part by the NSF CAREER Program CMS-9501470.

REFERENCES

1. R. L. CLARK, G. P. GIBBS and W. R. SAUNDERS 1998 *Adaptive Structures, Dynamics and Control*. New York: Wiley.
2. C. R. FULLER, S. J. ELLIOTT and P. A. NELSON 1996 *Active Control of Vibration*. San Diego: Academic Press.
3. P. A. NELSON and S. J. ELLIOTT 1992 *Active Control of Sound*. San Diego: Academic Press.
4. J. L. JUNKINS and Y. KIM 1993 *Introduction to Dynamics and Control of Flexible Structures*. Washington: AIAA.
5. P. DE FONSECA, P. SAS and H. VAN BRUSSEL 1999 *Journal of Sound and Vibration* **221**, 651–679. A comparative study of methods for optimizing sensor and actuator locations in active control applications.
6. G. C. SMITH and R. L. CLARK 1997 *American Institute of Aeronautics and Astronautics Paper* 97–1316. Optimal transducer placement for output feedback control of broadband structural acoustic radiation.
7. R. L. CLARK and D. E. COX 1999 *American Institute of Aeronautics and Astronautics Journal of Guidance, Control and Dynamics* **22**, 740–745. Band-limited actuator and sensor selection for disturbance rejection.
8. G. C. SMITH and R. L. CLARK 1999 *Proceedings of the Active* 99, *Fort Lauderdale, FL*, Poughkeepsie, NY: Noise Control Foundation. Adaptive structure design through optimal spatial compensation.
9. K. B. LIM 1997 *American Institute of Aeronautics and Astronautics Journal of Guidance, Control and Dynamics* **20**, 202–204. Disturbance rejection approach to actuator and sensor placement.
10. N. W. HAGOOD, W. H. CHUNG and A. VON FLOTOW 1990 *American Institute of Aeronautics and Astronautics Paper* 90-1087-CP. Modelling of piezoelectric actuators dynamics for active structural control.
11. K. B. LIM and W. GAWRONSKI 1996 *American Institute of Aeronautics and Astronautics Journal of Guidance, Control and Dynamics* **19**, 1370–1377. Hankel singular values of flexible structures in discret time.
12. W. GAWRONSKI and K. B. LIM 1996 *International Journal of Control* **65**, 131–145. Balanced actuator and sensor placement for flexible structures.
13. T. WILLIAMS 1990 *IEEE Transactions on Automatic Control* **35**, 379–382. Closed-form Grammians and model reduction for flexible space structures.
14. S. BOYD and C. BARATT 1991 *Linear Controller Design: Limits of Performance*, NJ: Prentice-Hall, Inc.
15. S. SKOGESTAD and I. POSTLEWAITE 1996 *Multivariable Feedback Control: Analysis and Design*. New York: Wiley.
16. W. C. DOYLE, K. GLOVER, P. P. KHARGONEKAR and B. A. FRANCIS 1989 *IEEE Transactions on Automatic Control* **AC-34**, 831–847. State-space solutions to standard $\mathscr{H}_2$ and $\mathscr{H}_2$ control problems.
17. J. S. VIPPERMAN and R. L. CLARK 1999 *Journal of Acoustical Society of America* **106**, 1392–1399. Implications of using colocated strain-based transducers for active structural acoustic control.
18. G. C. SMITH and R. L. CLARK 1999 *Journal of Sound and Vibration* **228**, 1182–1194. Tradeoffs in design complexity—temporal versus spatial compensation.
19. G. C. SMITH and R. L. CLARK 1999 *Noise Control Engineering Journal* **48**, 67–69. Performance measures for active control: passive insertion loss (PIL), active insertion loss (AIL) and total insertion loss (TIL).